Materials Today Communications 37 (2023) 107494

Contents lists available at ScienceDirect

Materials Today Communications

journal homepage: www.elsevier.com/locate/mtcomm

Modeling, spectroscopic structural properties of platinum-II complexes of 2-((phenylimino)methyl)phenolate-based ligands and research of nonlinear optical, organic light emitting diode and solar cell performances

Sultan Erkan, Duran Karakaş *

Cumhuriyet University, Science Faculty, Department of Chemistry, 50140 Sivas, Turkey

ARTICLE INFO

Keywords:
Schiff base complexes
NLO
OLED
SC

ABSTRACT

The hypothetical $Pt(B^1)_2$, $Pt(B^2)_2$ and $Pt(B^3)_2$ complexes were modeled. B^1, B^2 and B^3 are Schiff bases, 2-((phenylimino)methyl)phenolate, 4-methyl-2-((phenylimino)methyl)phenolate and 4-nitro-2-((phenylimino)methyl)phenolate, respectively. The ground state structures of the complexes were computed at the DFT-B3LYP/6–31 G(d)/LANL2DZ level. From the characteristic bond lengths, bond angles, bond stretching frequencies and proton chemical shift values, the platinum environment geometry was found to be square plane. The nonlinear optical (NLO) activities of the complexes were investigated by calculating some nonlinear optical property parameters and NLO performance of $Pt(B^3)_2$ was found to be higher than other complexes. Organic light emitting diode (OLED) performances of the complexes were investigated and found that the all complexes could be suitable for the production of OLED-featured materials. The solar cell (SC) performances of the complexes were determined by considering the power conversion efficiency (PCE). it was suggested that the $Pt(B^3)_2$ complex might have the highest solar cell performance.

1. Introduction

2-((phenylimino)methyl)phenolate ligand is a bidentate and negatively charged Schiff base ligand that can form complexes by binding to metals from N and O atoms. Schiff bases can be obtained through the reaction of ketones or aldehydes with primary amines [1], while Schiff base complexes can be synthesized from the reaction of Schiff bases with metal ions under moderate conditions [2]. Both Schiff base compounds and their metal complexes are of medical importance [3]. They are used in various fields of medicine as antifungal, antibacterial, antimalarial, antiproliferative, anti-inflammatory, antiviral, antipyretic and anticancer agents [4-6]. Four-coordinate and square-plane geometry coordination complexes are used as effective drugs against various diseases, especially cancer [7]. Transition metal complexes containing Schiff bases with N and O donor atoms are also used as inorganic catalysts [8–11]. The five coordinated ruthenium (II) carbonyl Schiff base complex was used as a catalyst to convert aldehydes to primary amides by M. Ramesh and G. Venkatachalam [12]. Recent studies reveal that Schiff base ligands and their coordination complexes can be compounds with NLO and OLED properties [13]. NLO materials have an important function in signal processing, modern communication technology, optical switches and optical memory devices [14]. The NLO activity of the molecules may be due to the freely moving π-electrons throughout the entire molecule. As the delocalization of the π-electrons increases, the NLO property increases. The donor-acceptor groups attached to the molecule may also result in increased mean linear polarizability and hyperpolarizability [15]. HOMO-LUMO energy gap is also one of the factors to be considered in order to produce materials with NLO properties. Therefore, UV-Vis spectra of molecules can be used to predict NLO properties [16,17].

Today, optoelectronic technology is becoming more and more widespread. For this reason, designing and synthesizing materials with OLED properties has been an important field of study. Because materials with OLED feature are widely used in fields such as photovoltaic devices, fluorescent switches, data storage, sensors, display, new generation light sources, security technology [18]. To design materials with excellent photo-physical properties, it is necessary to attach suitable substituents to the molecular structure that facilitate intramolecular charge transfer (ICT) [19–21]. Transition metal complexes of Schiff bases can exhibit OLED properties due to metal to ligand (ML), ligand to ligand (LL), ligand to metal (LM), and intra-ligand (IL) charge transfer [22].

It is also very important to design and synthesize photovoltaics or

* Corresponding author.
E-mail address: dkarakas@cumhuriyet.edu.tr (D. Karakaş).

https://doi.org/10.1016/j.mtcomm.2023.107494
Received 11 September 2023; Received in revised form 17 October 2023; Accepted 31 October 2023
Available online 3 November 2023

solar cells (SC) used to convert solar energy, which is an unlimited energy source, into electrical energy. Silicon-based inorganic materials are widely used in solar cell devices. Because they have high power conversion efficiency [23]. However, they also have some disadvantages such as being expensive, having a compact structure and being transparent [24].

In this work, we aimed to survey the design, characterization, NLO, OLED and SC properties of platinum-II complexes of 2-((phenylimino) methyl)phenolate-based Schiff bases. For this purpose, we formed B^1, B^2 and B^3 ligands by binding H, CH_3 and NO_2 substituents to the 4-position of the 2-((phenylimino)methyl)phenolate ligand, respectively. We designed $Pt(B^1)_2$, $Pt(B^2)_2$ and $Pt(B^3)_2$ complexes with these ligands. Structural characterization of the complexes was made with some structural parameters, IR and ^{1}H-NMR data calculated at the DFT-B3LYP/6–31 G(d)/LANL2DZ level. NBO, FMO, dipole moment (μ), mean linear polarizability (α) and first hyperpolarizability (β) calculations were performed to predict NLO properties. Transfer integrals (t_h and t_e), reorganization energies (λ_h and λ_e) for hole and electron were calculated to predict OLED performances. Band gap (E_g), maximum absorption wavelength (λ_{max}), oscillating strength (f_{os}), exciton binding energy (E_b), open circuit voltage (V_{oc}) and light harvesting efficiency (LHE) calculations were performed to estimate the SC performances of the complexes.

2. Computational procedure

Molecular structures of $Pt(B^1)_2$, $Pt(B^2)_2$ and $Pt(B^3)_2$ complexes were modeled with GaussView 6.0.16 program [25]. The structures were first optimized with the Ultra Force Field (UFF) method, a molecular mechanics method [26]. Then, full optimization was performed at the gas phase Gaussian 16: ES64L-G16RevC.01 program at the B3LYP/6–31 G (d)/LANL2DZ level [27] and no imaginer frequency was obtained [28]. Ground state structures, structural parameters and IR spectra for the complexes were obtained. ^{1}H-NMR spectra of the complexes were computed using the gauge-including atomic orbital (GIAO) approach to characterize the ground state structures of the complexes [29]. ^{1}H-NMR spectra and chemical shifts are obtained against the tetramethyl silane (TMS). Where, B3LYP is a hybrid density functional theory (DFT) method [30] and 6–31 G(d)/LANL2DZ is a mixed basis set. LANL2DZ basis set with effective core potential was used to model central atom platinum orbitals and the polarized basis set 6–31 G(d) was used to represent the orbitals of the other atoms [31]. To estimate the first hyperpolarizability, d polarization functions are added to the carbon and nitrogen atoms [32]. The reason for choosing the B3LYP/6–31 G (d)/LANL2DZ level is that it gives results that are quite compatible with the experimental values in the energy calculations of tetrazole type molecules and in the molecular structure calculations of metal-free phthalocyanines [33,34]. Various parameters were calculated at the B3LYP/6–31 G(d)/LANB2DZ level to predict the NLO, OLED and SC performances of the complexes.

3. Findings and discussion

3.1. Molecular structure characterization

Structures modeled in GaussView 6.0.16 program were optimized at the B3LYP/6–31 G(d)/LANL2DZ level in the gas phase for the obtaining the ground state structures. The optimized structures are given in Fig. 1.

The lengths of some characteristic bonds, bond angles and dihedral angles in $Pt(B^n)_2$ type complexes are given in Table 1.

As seen in Table 1, the bonding of the electron donor CH_3 and electron acceptor NO_2 groups to the 4-position of the 2-((phenylimino) methyl)phenolate Schiff base did not significantly change the bond lengths, bond angles and dihedral angles around the platinum atom. In the complexes, Pt-N lengths are 2.05, Pt-O lengths are 2.02, C═N lengths are 1.31, C-N lengths are 1.44 and C-O lengths are around 1.30 Å. In addition, N-Pt-O interior angles are around 92° and exterior angles are around 88°, which is quite close to the ideal square plane angle of 90°. N-Pt-N and O-Pt-O angles are 180° and are ideal trans angles. These findings show that the environment geometry of the central platinum atom is square plane. Dihedral angles also support this situation. The dihedral angles of Pt49-O2-C4-C7 and Pt49-N1-C3-H5 are very close to 180°, indicating that the phenolate rings and the central platinum atom are in the same plane. Whereas, the dihedral angles between the plane of the phenyl rings attached to the C═N group and the plane of the phenolate rings are around 67°. This finding indicates that the phenyl rings attached to the imine nitrogen are not in the same plane as the phenolate rings. The bond lengths and bond angles obtained in this study are quite consistent with the values obtained in our previous study [35]. In addition, the bond lengths, bond angles and dihedral angles on one side of the complexes are equal to those on the other side, indicating that the complexes have a center of symmetry.

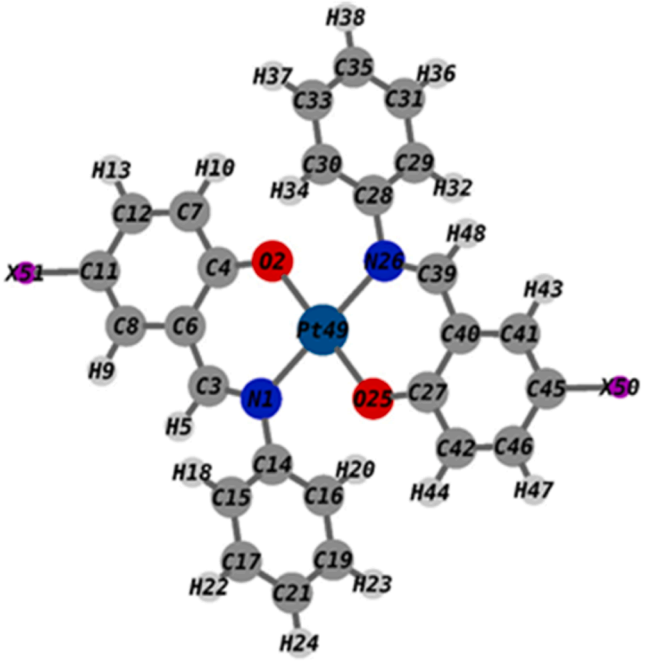

Fig. 1. Ground state structures and atom labeling of $Pt(B^n)_2$ complexes obtained at the B3LYP/6–31 G(d)/LANL2DZ level. where, X50 = X51 = H for $Pt(B^1)_2$, X50 = X51 = CH_3 for $Pt(B^2)_2$ and X50 = X51 = NO_2 for $Pt(B^3)_2$.

Table 1
Some characteristic bond lengths, bond angles and dihedral angles of $Pt(B^n)_2$ type complexes.

Bond Lengths (Å)	**Pt $(B^1)_2$**	**Pt $(B^2)_2$**	**Pt $(B^3)_2$**
Pt49-N1 = Pt49-N26	2.052	2.053	2.053
Pt49-O2 =Pt49-O25	2.022	2.022	2.020
N1-C3 =N26-C39	1.308	1.309	1.304
N1-C14 =N26-C28	1.438	1.438	1.442
O2-C4 =O25-C27	1.303	1.304	1.296
Bond angles (°)	**$Pt(B^1)_2$**	**$Pt(B^2)_2$**	**$Pt(B^3)_2$**
N1-Pt49-O2 =N26-Pt49-O25	92.2	92.2	92.1
N1-Pt49-O25 =N26-Pt49-O2	87.8	87.8	87.9
N1-Pt49-N26 = O2-Pt49-O25	180.0	180.0	180.0
C3-N1-Pt49 =C39-N26-Pt49	122.7	122.7	122.9
C4-O2-Pt49 =C27-O25-Pt49	126.7	126.5	127.0
Dihedral angles (°)	**$Pt(B^1)_2$**	**$Pt(B^2)_2$**	**$Pt(B^3)_2$**
Pt49-O2-C4-C7 =Pt49-O25-C27-C42	± 176.9	± 177.2	± 176.5
Pt49-N1-C3-H5 =Pt49-N26-C39-H48	± 178.2	± 178.3	± 178.1
Pt49-N1-C14-C16 =Pt49-N26-C28-C30	± 66.7	± 66.6	± 68.4

3.2. IR spectra and labeling of characteristic peaks

One of the most used techniques in molecular structure characterization is IR spectroscopy. In IR spectroscopy, it is checked whether there is a peak in the spectrum, belonging to the characteristic stretching for the molecule, and at what frequency the peak occurs. IR spectrums of the complexes designed in this study were calculated at the B3LYP/6–31 G(d)/LANL2DZ level. No imaginary frequency was obtained as a result of the calculation. Therefore, the complexes are in the ground state and have the lowest energy. IR spectra of the complexes, the frequencies of the characteristic peaks and their labeling are presented in Fig. 2.

As seen in Fig. 2, the characteristic C═N stretching peaks for the complexes were calculated in the range of 1650–1675 cm^{-1}, the C-O stretching peaks were in the range of 1365–1373 cm^{-1} and the C-H stretching peaks in the imine group were around 3140–3150 cm^{-1}. Experimentally, C═N stretching peaks were found in the range of 1594–1612 cm^{-1} and C-O stretching peaks were found around 1303–1310 cm^{-1} in ruthenium complexes of similar ligands [12]. No scale factor has been found in the literature that can be used to convert the frequencies calculated at the B3LYP/6–31 G(d)/LANL2DZ level into anharmonic frequencies. However, the scale factor is given as 0.952 for the B3LYP/6–31 G(d) level [36]. Considering that this level is close to our working level, it is seen that the calculated C═N and C-O frequencies are compatible with the experimental values. The fact that the frequencies of the calculated characteristic peaks are compatible with the frequencies of similar synthesized complexes shows that the designed complexes will be stable and synthesizable. Since the peak frequency is directly proportional to the square root of the bond force constant, this result also shows that the bond force constants are compatible.

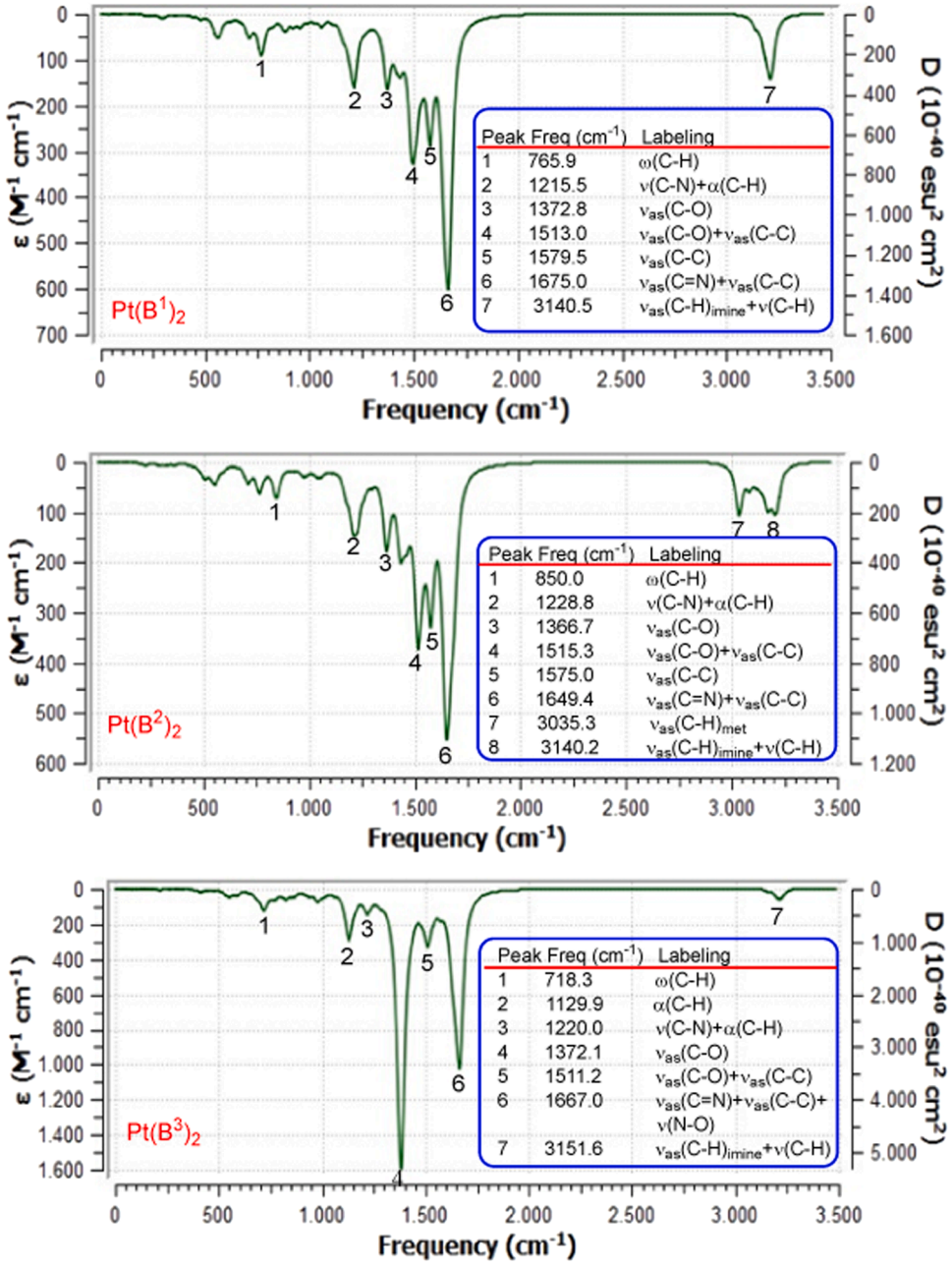

Fig. 2. IR spectrums of $Pt(B^n)_2$ type complexes calculated at B3LYP/6–31 G(d)/LANL2DZ level and labeling of characteristic peaks. (ω:Wagging, α: Scissoring, ν: stretching, νas: asymmetric stretching, met: methyl).

3.3. ^{1}H-NMR spectra and chemical shifts

One of the most widely used methods to determine molecular structures is nuclear magnetic resonance (NMR) spectroscopy. With this spectroscopic method, the ^{1}H-NMR and ^{13}C-NMR chemical shifts of the molecule are measured and the results are usually given according to the TMS reference. Important information about molecular structure can be obtained from these data. ^{1}H-NMR spectra of the designed $Pt(B^{n})_2$ complexes in this study were computed at the B3LYP/6–31 G(d)/LANL2DZ level by GIAO method. The shielding value for TMS protons at the same level was found to be 32.2001 ppm. ^{1}H-NMR chemical shifts were obtained from Eq. (1).

$$\delta_H = \sum H_{TMS} - \sum H_{sample} \quad (1)$$

where, ΣH_{TMS} is shielding of TMS protons and ΣH_{sample} is shielding of sample protons. ^{1}H-NMR spectra of the Schiff base complexes, the labeling of the peaks and ^{1}H-NMR chemical shifts are given in Fig. 3.

As can be seen in Fig. 3, the chemical shifts of the protons bonded to the aromatic ring in all three complexes are around 6–8 ppm and the chemical shifts of the aliphatic CH_3 protons in $Pt(B^{2})_2$ complex are around 1–2 ppm. The H5, H48 protons in the CH=N groups peaked at 7.76 ppm in the $Pt(B^{1})_2$ and $Pt(B^{2})_2$ complexes and at 7.94 ppm in the $Pt(B^{3})_2$ complex. In the ruthenium complexes of a similar ligand, N-salicylidene-2-hydroxyaniline Schiff base, the chemical shifts of the protons bonded to the aromatic carbons were experimentally found to be between 6 and 8 ppm and the CH=N group protons in the range of 8.9–9.2 ppm [37]. These data appear to be in fairly good agreement.

As seen in Fig. 3, some of the protons are equivalent. For example, in $Pt(B^{1})_2$, the protons H10 and H44 and H50 and H51 are equivalent to each other. Because they have the same chemical shift. As can be seen in

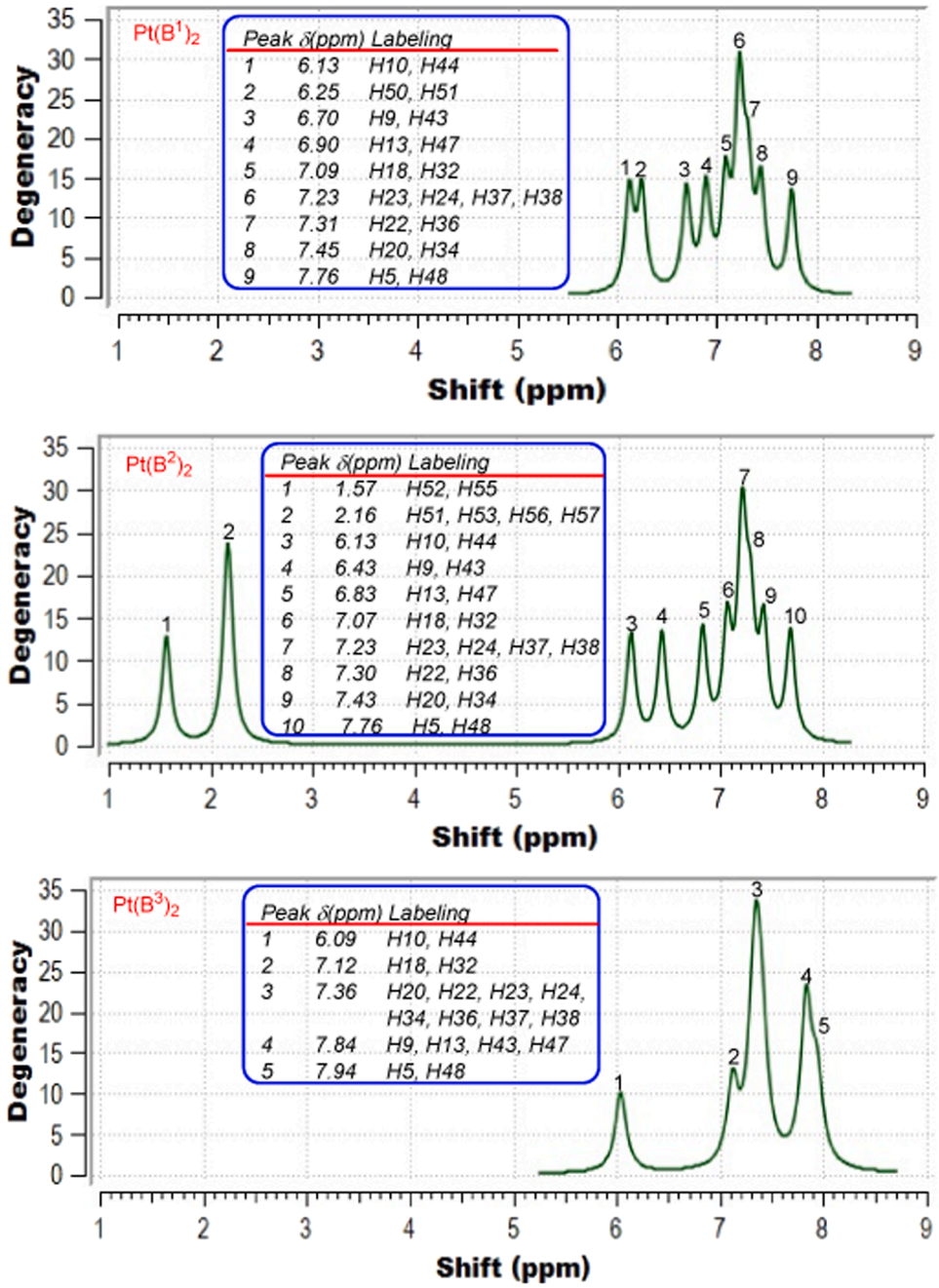

Fig. 3. ^{1}H-NMR spectrums of $Pt(B^{n})_2$ complexes computed at B3LYP/6–31 G(d)/LANB2DZ level by GIAO model and labeling of peaks.

Fig. 1, these protons are in a trans position with each other. These findings show that all three complexes have a square plane geometric structure and Schiff base ligands are in trans position with respect to each other.

3.4. Natural bond orbital analyzes

Various methods such as natural bond orbital analysis, frontier molecular orbital analysis, mean linear polarizability calculations and first hyperpolarizability calculations can be considered to estimate the NLO performances of molecules. In order to estimate the NLO performance with NBO analysis, the electron delocalization between the occupied bond orbital or the non-bonding orbital (donor) and the unoccupied anti-bonding orbital (acceptor) can be calculated quantitatively from equation (2) [38].

$$E(2) = \Delta E_{ij} = q_i \frac{F_{ij}^2}{E_j - E_i} \quad (2)$$

where, E(2) is the interaction energy or stability energy, qi is the occupancy rate of the ith donor orbital, Fij is the off-diagonal NBO Fock matrix element, and E_j and E_i are the energies of the j and i orbitals. A greater stability energy indicates there are the higher interaction between donor and acceptor species and more conjugation over the entire system [39]. Increasing of electron conjugation in the molecule increases the NLO property of the molecule. In this study, E(2) energies between the same donor-acceptor species in $Pt(B^n)_2$ complexes were computed at the B3LYP/6–31 G(d)/LANL2DZ level and are their values are presented in Table 2.

As can be seen from Table 2, the largest E(2) energies are between the types BD* (2)(C27-C40)→BD* (2)(C41-C45) and BD* (2)(C27-C40)→(C42-C46). This result indicates that there is significant conjugation between these species. To predict the total conjugation in the complexes, the total stability energies between the same donor-acceptor species were calculated and are given in the last row of Table 2. According to the total E(2) energies, the order of conjugation in the complexes is $Pt(B^2)_2 < Pt(B^1)_2 < Pt(B^3)_2$. In the $Pt(B^3)_2$ complex, the electron acceptor NO_2 group is attached at the 4-position of the 2-((phenylimino)methyl)phenolate Schiff base. According to this finding, it can be said that the electron acceptor NO_2 group increases the electron conjugation and NLO properties of the $Pt(B^3)_2$ complex.

3.5. Dipole moment, polarizability and hyperpolarizability calculations

One of the methods used to estimate the NLO performances of molecules is to calculate their dipole moment (μ), polarizability (α) and hyperpolarizability (β) values. The relationship between these parameters and NLO performance is given by the Taylor equation [40].

$$E = E_0 - \mu_i F_i - \frac{1}{2}\alpha_{ij}F_iF_j - \frac{1}{6}\beta_{ijk}F_iF_jF_k - \ldots \quad (3)$$

Table 2
Calculated stability energies at the B3LYP/6–31 G(d)/LANL2DZ level between the same donor-acceptor species in $Pt(B^n)_2$ complexes.

		E (2) (kcal/mol)		
Donor(i)	Acceptor(j)	$Pt(B^1)_2$	$Pt(B^2)_2$	$Pt(B^3)_2$
BD(2) (C27-C40)	BD* (2) (N26-C39)	34.62	34.79	31.93
BD* (2) (N26-C39)	BD* (2) (C27-C40)	79.40	77.77	94.66
BD* (2) (C27-C40)	BD* (2) (C41-C45)	175.38	124.11	251.98
BD* (2) (C27-C40)	BD* (2) (C42-C46)	173.51	182.63	111.39
LP(2) (O25)	BD* (2) (C27-C40)	55.13	54.85	56.65
LP(3) (O25)	LP* (5) (Pt49)	71.78	71.90	68.56
LP(3) (O25)	LP* (6) (Pt49)	66.39	66.49	65.73
LP(1) (N26)	LP* (5) (Pt49)	96.97	96.93	99.52
LP(1) (N26)	LP* (6) (Pt49)	67.73	67.74	66.34
	Total E(2)	820.91	777.21	846.76

Where, E is the energy of the molecule in the F electric field, E_0 is the energy in the absence of any electric field acting on the molecule, F_i is the electric field strength applied to the molecule in the i direction, μ_i is the static dipole moment of the molecule in the i direction, α_{ij} is the mean linear polarizability of the molecule, and β_{ijk} is indicates the first hyperpolarizability of the molecule. The μ, α and β values in Taylor equation can be calculated from the Gaussian output file using the following equations [41,42].

$$\mu = \left(\mu_x^2 + \mu_y^2 + \mu_z^2\right)^{1/2} \quad (4)$$

$$|\alpha| = \frac{1}{3}(\alpha_{xx} + \alpha_{yy} + \alpha_{zz}) \quad (5)$$

$$\beta = \left[(\beta_{xxx} + \beta_{xyy} + \beta_{xzz})^2 + (\beta_{yyy} + \beta_{yzz} + \beta_{yxx})^2 + (\beta_{zzz} + \beta_{zxx} + \beta_{zyy})^2\right]^{1/2} \quad (6)$$

As seen from the Taylor equation, the lower the E energy of a molecule in the F electric field, the higher the NLO activity. In such studies, rather than comparing the E energies of the molecules, the μ, α and β values of the molecules are compared with the values of the urea used as a reference. The larger the μ, α and β values calculated for the molecules, the higher the NLO activity of the molecule. The components α and β taken from the Gaussian output file are given in atomic unit (a.u). The results are converted to esu by using the conversion factors 1a.u= 1.482×10^{-25} esu for α and 1a.u= 8.639×10^{-33} esu for β [41]. The μ, α and β values of $Pt(B^n)_2$ complexes modeled in this study and urea used as a reference were computed from the Eqs. (4)–(6) and given in Table 3.

As seen from Table 3, the μ, α and β values of the $Pt(B^3)_2$ complexes are higher than those of the other complexes. This data indicates that the NLO activity of the $Pt(B^3)_2$ complex may be higher than that of the other complexes. It can be said that NO_2 group in the $Pt(B^3)_2$ complex creates a good conjugation effect by attracting the π-electrons of the benzene ring with its strong electron withdrawing ability and increases the NLO activity. However, the fact that μ and β values of the complexes are smaller than those of urea may mean that they may not be suitable for NLO material.

3.6. Frontier molecular orbital analyzes

The highest occupied molecular orbital (HOMO) and the lowest unoccupied molecular orbital (LUMO) are known as frontier molecular orbitals (FMO). Energy gap (E_g) between the FMOs can also be used to predict the NLO performances of molecules. Energy gap between the FMOs can be calculated from Eq. (7).

$$E_g = E_{LUMO} - E_{HOMO} \quad (7)$$

As the energy gap of the molecule decreases, polarizability and electron delocalization increase [16]. Increasing the polarizability and electron delocalization causes the NLO property to increase. In this work, the energy gap was calculated from Eq. (7) to predict the NLO properties of $Pt(B^n)_2$ complexes. Contour diagrams, energies and energy gaps of the FMOs are given in Fig. 4.

As seen in Fig. 4, LUMO is concentrated on the platinum atom in all of the complexes. This orbital is predominantly the d^2_{xy} orbital of the central platinum atom. While, HOMO orbital in the $Pt(B^1)_2$ complex is

Table 3
μ, α and β values of $Pt(B^n)_2$ complexes and urea.

Parameter	$Pt(B^1)_2$	$Pt(B^2)_2$	$Pt(B^3)_2$	Urea
μ (D)	0.0008	0.0008	0.0012	4.2671
$\alpha x10^{-25}$ (esu)	263.88	281.04	364.78	32.581
$\beta x10^{-33}$ (esu)	0.0466	0.1881	1.3076	138.19

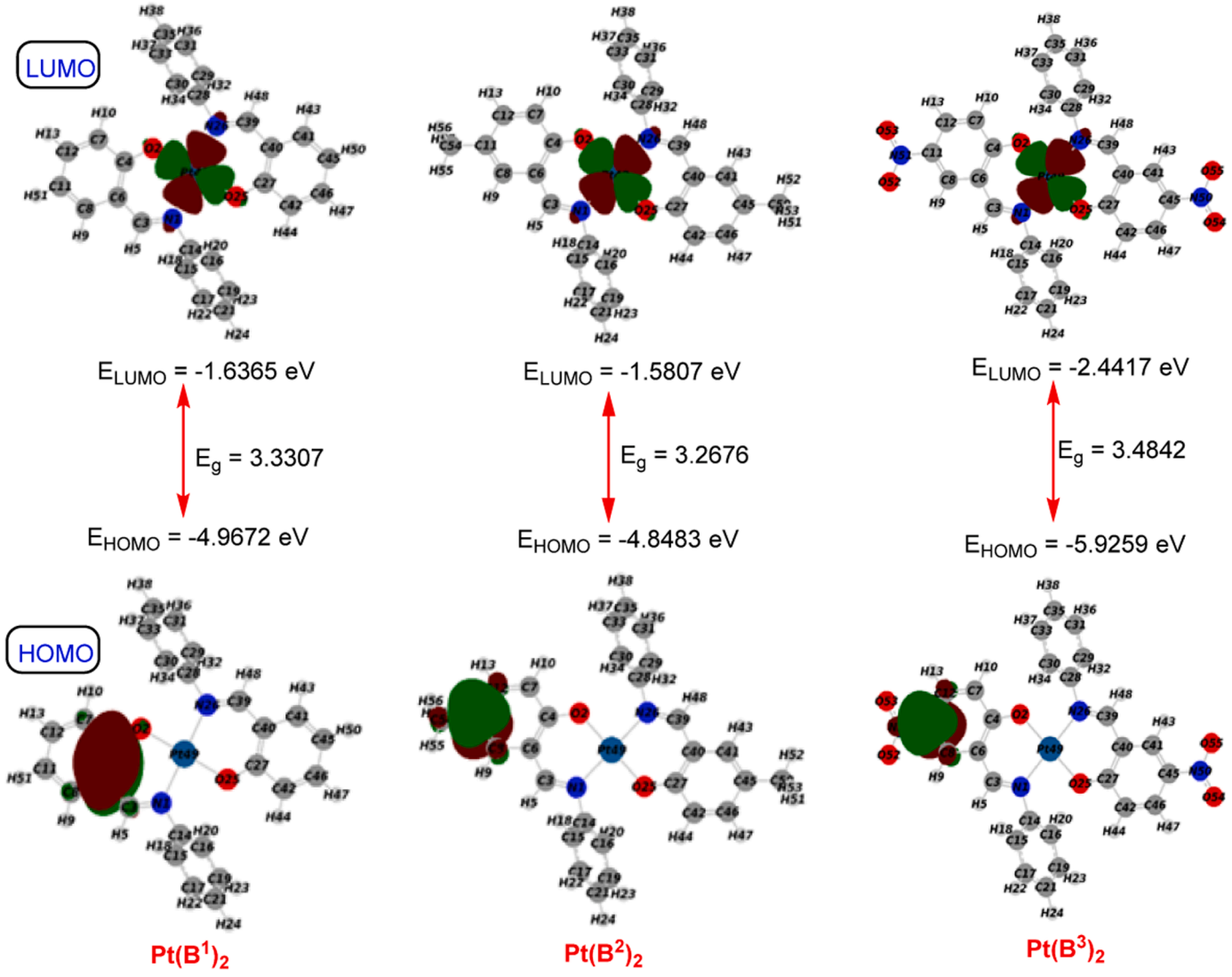

Fig. 4. Contour diagrams, energies and energy gaps of the FMOs of $Pt(B^n)_2$ complexes obtained at the B3LYP/6–31 G(d)/LANL2DZ level.

the π-molecular orbital on the C3-C6-C4 atoms and HOMO orbital in the $Pt(B^2)_2$ and $Pt(B^3)_2$ complexes are the π-molecular orbital on the C8-C11-C12 atoms. $Pt(B^2)_2$ complex has the lowest energy gap, while $Pt(B^3)_2$ complex has the highest energy gap. It can be said that the NLO property of the $Pt(B^2)_2$ complex will be higher, as the NLO property will increase as the energy gap decreases. This result indicates that electron donating species such as CH_3 decrease the energy gap and increase the NLO property.

The NLO performance ranking of the complexes according to the calculated stability energies (E2), static dipole moment (μ), mean linear polarizability (α), first hyperpolarizability (β) and energy gaps (E_g) is as follows.

E(2): $Pt(B^2)_2 < Pt(B^1)_2 < Pt(B^3)_2$.
μ: $Pt(B^1)_2 = Pt(B^2)_2 < Pt(B^3)_2$.
α: $Pt(B^1)_2 < Pt(B^2)_2 < Pt(B^3)_2$.
β: $Pt(B^1)_2 < Pt(B^2)_2 < Pt(B^3)_2$.
E_g: $Pt(B^3)_2 < Pt(B^1)_2 < Pt(B^2)_2$.

It is seen from most of these ranking that the NLO property of the $Pt(B^3)_2$ complex is higher than the other complexes. However, since the μ and β values of the complexes are lower than the reference urea, it can be said that they are not very suitable for the production of materials with NLO properties. It can be seen that the ranking made according to E_g values is quite different from the others. In this study, we used the B3LYP functional to calculate HOMO and LUMO energies. It is well known that such functionals severely underestimate HOMO and LUMO energies and provide inaccurate polarizability [43,44]. Using newer range-separated functionals such as CAM-B3LYP, LC-BLYP and methods such as CCSD instead of traditional hybrid DFT methods in calculating HOMO, LUMO energies and polarizabilities may provide more accurate results.

3.7. Organic light emitting diode performances

Marcus theory can be used to theoretically predict the organic light emitting diode (OLED) properties of molecules. According to Marcus theory, the charge transfer rate between adjacent segments in molecules is given by the following equation [45].

$$k_{CT} = \frac{2\pi}{\hbar} t^2 \sqrt{\frac{1}{4\pi\lambda k_B T}} \exp\left[-\frac{(\lambda + \Delta G^0)^2}{4\lambda k_B T}\right] \quad (8)$$

In this equation, k_{CT} is the rate of charge transfer, t is the charge transfer integral for the electron or hole, ħ is the reduced Planck constant, λ is the internal reorganization energy for the electron or hole, k_B is the Boltzmann constant, T is the temperature, and ΔG^0 is the Gibbs free energy of the charge transfer reaction. As seen from Eq. (8), the rate of charge transfer depends on the charge transfer integral (t) and the reorganization energy (λ). There are several methods for calculating

charge transfer integrals in molecules. One of them is based on Koopman's theorem. According to Koopman's theorem, charge transfer integrals for electron and hole can be calculated from the following equations [46].

$$t_e = \frac{1}{2}(E_{LUMO+1} - E_{LUMO}) \quad (9)$$

$$t_h = \frac{1}{2}(E_{HOMO} - E_{HOMO-1}) \quad (10)$$

As can be seen from the Marcus equation, another important parameter affecting the charge transfer rate is the reorganization energy, which represents the geometric relaxation accompanying the charge transfer. The reorganization energy for electron (λ_e) and hole (λ_h) in isolated molecular systems can be calculated from the following equations using the single point energies of neutral, cationic and anionic species [47].

$$\lambda e = \left(E_0^- - E_-^-\right) + \left(E_-^0 - E_0^0\right) \quad (11)$$

$$\lambda_h = \left(E_0^+ - E_+^+\right) + \left(E_+^0 - E_0^0\right) \quad (12)$$

Where, E_0^+ and E_0^- are the energies of cation and anion formed from neutral molecule, E_+^+ and E_-^- are the energies of cation and anion formed from cation and anion, E_+^0 and E_-^0 are the energies of neutral molecules formed from cation and anion and E_0^0 is the ground state energy of the neutral molecule.

Other parameters used to predict the OLED activity of molecules are ionization potential (IP), electron affinity (EA) and chemical hardness (η). These parameters are easily calculated by Eqs. (13)-(15) [48].

$$IP = E_+^+ - E_0^0 \quad (13)$$

$$EA = E_0^0 - E_-^- \quad (14)$$

$$\eta = (IP - EA)/2 \quad (15)$$

In this work, $Pt(B^n)_2$ type complexes, electron reorganization energy reference mer-Alq_3 [tris (8-hydroxyquinolinato) aluminum (III)] [49] and hole reorganization energy reference TPD [N,N′-diphenyl-N,N′-bis (3-methlphenyl)-(1,1′-biphenyl)– 4,4′-diamine] [50] were optimized at the DFT/B3LYP/6–31 G(d)/LANL2DZ level of theory with the Gaussian 16:RevC.01 program. By taking the energies of the frontier molecular orbitals from these optimized structures, charge transfer integrals were calculated from Eqs. (9)-(10) according to Koopman's theorem for electrons and holes. To save time, the E_0^0, E_0^+, E_+^+, E_+^0, E_0^-, E_-^-, E_-^0 single point energies of the molecules were calculated at the DFT/B3LYP/MIDXL level in the Maestro Material Science program [51]. Reorganization energies for electron and hole (λ_e and λ_h), ionization potentials (IP) and electron affinities (EA) and chemical hardness (η) of the complexes and references were calculated from Eqs. (11)-(15). The calculated OLED parameters for complexes and references are given in Table 4.

As seen from the Marcus equation, at a given temperature, the rate of charge transfer (k_{CT}) is directly proportional to the square of the charge transfer integral (t^2) and as the value of the charge transfer integral increases, the charge transfer rate increases. As can be seen from Table 4, the values of both the hole transfer integrals (t_h) and electron transfer integrals (t_e) of the $Pt(B^n)_2$ complexes are significantly large. Also, the hole transfer integrals of the complexes are larger than the electron transfer integrals. Therefore, hole transfer integrals contribute significantly to the charge transfer rate. In addition, it can be said that the OLED performance of $Pt(B^1)_2$ will be higher due to its high electron transfer integral and hole transfer integral, and $Pt(B^3)_2$ due to its high hole transfer integral.

Generally, in OLED studies, mer-Alq_3 is used as the electron reorganization energy reference and TPD is used as the hole reorganization energy reference. In order to make comparisons with references, the reorganization energies of the references and complexes should be calculated at the same level. A. Lukyanov et al. calculated the reorganization energies of Alq_3 as λ_e= 0.28 and λ_h= 0.23 eV at B3LYP/6–311 G+ (dp) level [49]. In this study, the reorganization energies of mer-Alq_3 were calculated as λ_e= 0.319 and λ_h= 0.243 eV at B3LYP/-MIDXL level. B. C. Lin et al. calculated the reorganization energies for TPD at the B3LYP/6–31 G(d) level as λ_e= 0.561 and λ_h= 0.281 eV [50]. In this study, the reorganization energies for TPD were calculated as λ_e= 0.542 and λ_h= 0.263 eV at B3LYP/MIDXL level. Although these values are calculated at different levels, they are in agreement with each other.

As can be seen from the Marcus equation, the charge transfer rate increases as the reorganization energies decrease. Therefore, if the reorganization energies of the materials are lower than the reorganization energies of the references, it can be said that the material can have OLED properties. If $\lambda_e < \lambda_h$ for a material, the material can be considered as an electron carrier, and if $\lambda_h < \lambda_e$, the material can be considered as a hole carrier [52].

As seen in Table 4, the electron reorganization energies (λ_e) of all of the complexes are lower than the reference mer-Alq_3. This result indicates that the OLED performance of the complexes is more favorable than that of mer-Alq3. In addition, the lower electron reorganization energy of $Pt(B^3)_2$ indicates that electron withdrawing species may increase OLED properties.

Table 4
OLED parameters of $Pt(B^n)_2$ complexes and references Alq_3 and TPD.

Parameters	$Pt(B^1)_2$	$Pt(B^2)_2$	$Pt(B^3)_2$	Mer-Alq_3	TPD
E_{LUMO+1} (a.u)	-0.05066	-0.04877	-0.08061	-0.05499	-0.01125
E_{LUMO} (a.u)	-0.06014	-0.05809	-0.08973	-0.06358	-0.02854
t_e (eV)	0.129	0.127	0.124	0.117	0.235
E_{HOMO} (a.u)	-0.18254	-0.17817	-0.21777	-0.18399	-0.17189
E_{HOMO-1} (a.u)	-0.20936	-0.20306	-0.24491	-0.19208	-0.18688
t_h (eV)	0.365	0.339	0.369	0.110	0.204
E_0^0 (a.u)	-1374.730575	-1452.904101	-1781.475547	-1664.145745	-1567.659671
E_0^- (a.u)	-1374.734898	-1452.917277	-1781.515959	-1664.158630	-1567.646479
E_-^- (a.u)	-1374.740687	-1452.923065	-1781.521571	-1664.164462	-1567.657283
E_-^0 (a.u)	-1374.725063	-1452.898613	-1781.470647	-1664.139862	-1567.650562
λ_e (eV)	0.307	0.307	0.286	0.319	0.542
E_0^+ (a.u)	-1374.503424	-1452.682935	-1781.221172	-1663.911813	-1567.449181
E_+^+ (a.u)	-1374.506377	-1452.685620	-1781.225435	-1663.915430	-1567.453709
E_+^0 (a.u)	-1374.727382	-1452.901337	-1781.472695	-1664.140432	-1567.654517
λ_h(eV)	0.167	0.148	0.194	0.243	0.263
IP (eV)	6.101	5.945	6.806	6.267	5.604
EA (eV)	0.275	0.516	1.252	0.509	-0.065
η (eV)	5.826	5.429	5.553	5.758	5.669

As can be seen from Table 4, the hole reorganization energy (λ_h) of all of the complexes is lower than the reference TPD. According to their hole reorganization energies, the complexes can be used as materials with OLED properties. In addition, it appears that the hole reorganization energy of the $Pt(B^2)_2$ complex is lower. Therefore, it can be said that the electron donor groups in the ligands may increase the OLED properties by decreasing the hole reorganization energy. Since all of the complexes have $\lambda_h < \lambda_e$, the complexes can be taken into account as hole transport materials. As a result, it can be said that complexes can be materials with OLED properties from the reorganization energies calculated for electron and hole.

Since the chemical hardness of the molecules can be calculated from the IP and EA values, they are important parameters for predicting OLED properties. It is seen from Eq. (15) that molecules with lower IP and higher EA will have lower hardness. Chemical hardness is considered as a reference for estimating resistance in the intramolecular charge transfer process. Low chemical hardness means low resistance in the intramolecular charge transport process. Therefore, molecules with low hardness should have high OLED performances. As seen in Table 4, the hardness of $Pt(B^2)_2$ and $Pt(B^3)_2$ complexes is lower than both mer-Alq_3 and TPD. Therefore, it can be said that $Pt(B^2)_2$ and $Pt(B^3)_2$ complexes have higher OLED properties than $Pt(B^1)_2$ complexes.

3.8. Photovoltaic (solar cell) performance

The molecules to be used in photovoltaic or solar cell (SC) technology should have a high performance in converting sunlight into electrical energy. Parameters such as energy gap (E_g), maximum absorption wavelength (λ_{max}), oscillator strength (f_{os}), exciton binding energy (E_b), and power conversion efficiency (PCE) are generally used to evaluate the photovoltaic performance of molecules. The power conversion efficiency of a photovoltaic system can be determined by Eq. (16) [53].

$$PCE = \frac{V_{oc} \quad J_{sc}FF}{P_{inc}} \tag{16}$$

Where, V_{oc} is the open circuit voltage, J_{sc} is the short circuit current density, FF is the filling factor and P_{inc} is the incident solar energy. According to this equation, the power conversion efficiency of a photovoltaic system is directly proportional to V_{oc}, J_{cs} and FF. The higher their value, the higher the conversion performance. The V_{oc} value can be determined computationally by Eq. (17).

$$V_{oc} = |E_{HOMO}|_{sample} - |E_{LUMO}|_{reference} - 0.3 \tag{17}$$

In such studies, $PC_{61}BM$ (Phenyl-C_{61}-butyric acid methyl ester) is generally used as a reference. The energy of the conduction band of $PC_{61}BM$ is taken as $E_{LUMO} = -4.3$ eV [54]. In this study, we calculated the E_{LUMO} value for PC61BM as -3.145 eV at the B3LYP/6–31 G(d) level. This value is in good agreement with the value calculated by Bedoura et al. [55]. The short circuit current density (J_{sc}) in Eq. (16) is related to the energy gap (E_g) and the light harvesting efficiency (LHE). Molecules with a low energy gap have a high J_{sc} value [56]. Light harvesting efficiency (LHE) can be calculated from Eq. (18) [57].

$$LHE = 1 - 10^{-f_{os}} \tag{18}$$

Where, f_{os} is the oscillatory strength of the λ_{max} value in the absorption spectrum of the sample. The higher the oscillator strength, the higher the light harvesting efficiency. As the light harvesting efficiency increases, the power conversion efficiency of the solar cell system increases. The filling factor (FF) in Eq. (16) is related to the energy gap (E_g). Molecules with a low energy gap have a high filling factor [56]. A high filling factor increases the power conversion efficiency.

One of the vital parameters to be considered in estimating the photovoltaic performance of molecules is exciton binding energy (E_b) and is calculated from Eq. (19).

$$E_b = E_g - E_{opt} \tag{19}$$

Where E_b is the exciton binding energy, E_g is the energy gap and E_{opt} is the excitation energy. E_{opt} is commonly known as the first excitation energy and is the difference between the ground state energy (S_0) and the first excited singlet state energy (S_1). Molecules with low exciton binding energy generally have high PCE, J_{sc} and FF values [56].

Parameters such as maximum absorption wavelength (λ_{max}), oscillator strength (f_{os}), light harvesting efficiency (LHE) and exciton binding energy (E_b) are related to the electronic spectra of molecules. Therefore, the electronic absorption (UV-Vis) spectra of the complexes were calculated on the basis of time-dependent density functional theory at the TD-DFT/B3LYP/6–31 G(d)/LANB2DZ level [58] and are given in Fig. 5.

As seen in Fig. 5, three bands were obtained in the UV-Vis spectrum of each of the complexes. Labeling and wavelengths of the bands are given in Fig. 5. The absorption coefficient and oscillator strength of the 2nd band in $Pt(B^1)_2$ and $Pt(B^2)_2$ complexes, and the 1st band in the $Pt(B^3)_2$ complex are higher than those of the other bands. In all of the complexes, the 3rd band has the maximum wavelength (λ_{max}). In order to predict the solar cell performance of the complexes, properties such as the wavelength, orbital contribution, oscillator strength of the band that emerge at the maximum wavelength (λ_{max}) are important. In this study, E_{HOMO}, E_{LUMO}, E_g, λ_{max}, V_{oc}, LHE and E_b parameters were calculated to estimate the solar cell performances of the complexes and the values of these parameters are given in Table 5.

As seen in Table 5, λ_{max} values for $Pt(B^1)_2$, $Pt(B^2)_2$ and $Pt(B^3)_2$ are

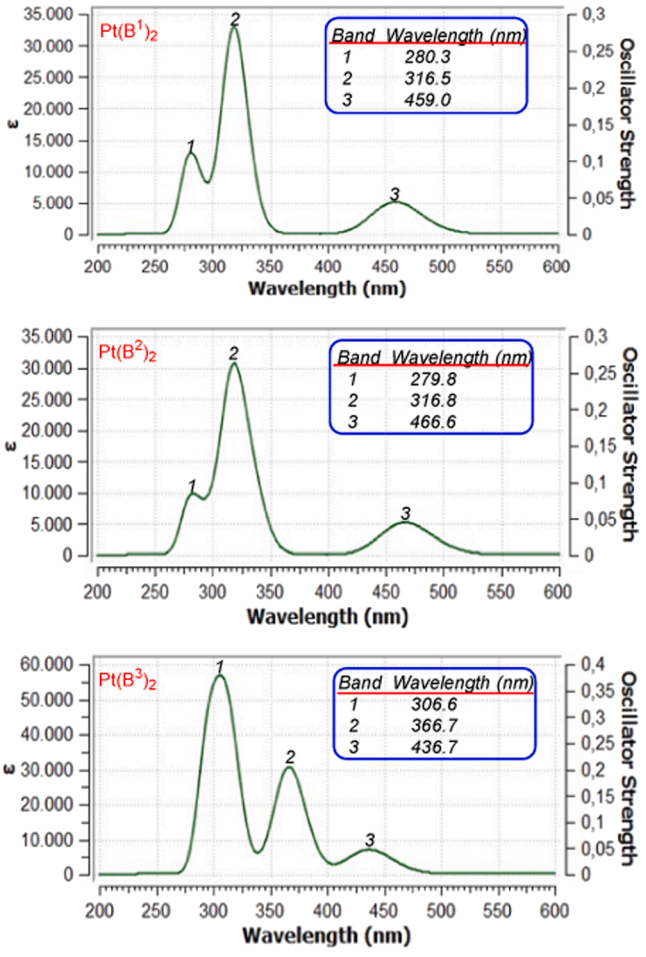

Fig. 5. Computed UV-Vis absorption spectrums of $Pt(B^n)_2$ complexes in gas phase at TD-B3LYP/6–31 G(d)/LANL2DZ level.

Table 5
Some solar cell performance parameters of $Pt(B^n)_2$ type complexes calculated in gas phase at TD-B3LYP/6–31 G(d)/LANL2DZ level.

Parameter	$Pt(B^1)_2$	$Pt(B^2)_2$	$Pt(B^3)_2$
E_{HOMO} (eV)	-4.9672	-4.8483	-5.9259
E_{LUMO} (eV)	-1.6365	-1.5807	-2.4417
E_g (eV)	3.3307	3.2676	3.4842
λ_{max} (nm)	459.0	466.6	436.7
Assignment	HOMO→LUMO	HOMO→LUMO	HOMO→LUMO
Contribution	0.701	0.700	0.695
V_{oc} (eV)	1.522	1.403	2.481
f_{os}	0.0562	0.0571	0.0770
LHE	0.121	0.123	0.162
E_{opt} (eV)	2.095	2.060	2.110
E_b (eV)	1.236	1.208	1.374

459.0, 466.6 and 436.7 nm, respectively. According to these values, λ_{max} values for all of the complexes fall into the visible region. As can be seen from the orbital contributions in Table 5, the bands in λ_{max} are mainly composed of HOMO→LUMO electronic transitions.

As can be seen from Eq. (17), the open circuit voltage (V_{oc}) in solar cells depends on the sample HOMO energy. As the absolute value of the sample HOMO energy increases, the V_{oc} and thus the PCE increase. As seen in Table 5, the PCE ranking according to HOMO energy is as follows.

E_{HOMO}: $Pt(B^2)_2 < Pt(B^1)_2 < Pt(B^3)_2$.

The energy gap is calculated using the HOMO and LUMO energies. Energy gap plays a vital role in estimating the PCE of solar cells, which is associated with the charge transfer process. Molecules with narrow energy gap have higher FF and J_{sc} values [58]. As FF and J_{sc} values increase, PCE increases. The PCE ranking of the complexes according to the energy gap is as follows.

E_g: $Pt(B^3)_2 < Pt(B^1)_2 < Pt(B^2)_2$.

Other factors to consider in estimating PCE are V_{oc} and LHE. As V_{oc} and LHE values increase, PCE increases. The PCE ranking of the complexes according to these values is as follows.

V_{oc}: $Pt(B^2)_2 < Pt(B^1)_2 < Pt(B^3)_2$.

LHE: $Pt(B^1)_2 < Pt(B^2)_2 < Pt(B^3)_2$.

As explained above, molecules with low exciton binding energy (E_b) have high PCE value. E_{opt} values of the complexes were calculated in Schrödinger Maestro Material Science program and exciton binding energies were obtained from Eq. (19). The PCE order of the complexes according to the exciton binding energy is as follows.

E_b: $Pt(B^3)_2 < Pt(B^1)_2 < Pt(B^2)_2$.

According to the E_{HOMO}, V_{oc} and LHE parameters, the PCE value of the $Pt(B^3)_2$ complex was higher than the other complexes. As seen in Table 5, the presence of electron acceptor NO_2 group in the $Pt(B^3)_2$ complex decreased the HOMO energy. The decrease in HOMO energy increased the PCE parameter and solar cell performance.

4. Conclusions

In this study, hypothetical $Pt(B^1)_2$, $Pt(B^2)_2$ and $Pt(B^3)_2$ complexes were modeled. The complexes were optimized at the DFT-B3LYP/6–31 G(d)/LANL2DZ level. From the characteristic bond lengths, bond angles, characteristic bond stretching frequencies in the IR spectra and ^{1}H-NMR chemical shifts for the complexes, the platinum environment geometry was found to be square plane. The NLO performances of the complexes were investigated according to the calculated stability energies (E2), static dipole moment (μ), mean linear polarizability (α), first hyperpolarizability (β) and energy gap (E_g) values. Since the μ and β parameters of the complexes were lower than those of the reference urea, it was estimated that they may not be very suitable for NLO material production. Transfer integrals and reorganization energies were calculated for the OLED performances of the complexes. From the calculated transfer integrals and reorganization energies, it was predicted that the complexes could be used as materials with OLED properties. The power conversion efficiency (PCE) of the complexes was estimated using open circuit voltage (V_{oc}), short circuit current density (J_{sc}), filling factor (FF), light harvesting efficiency (LHE), energy gap (E_g) and exciton binding energy (E_b) calculations. According to the PCE evaluation made here, the solar cell performance of the $Pt(B^3)_2$ complex was predicted to be better than the other complexes.

CRediT authorship contribution statement

Sultan Erkan: To predict the NLO, OLED and SC performances of complexes, performing the calculations such as natural bond orbital, mean linear polarizability, first hyperpolarizability, frontier molecular orbital energies, transfer integrals, reorganization energies, open circuit voltage, light harvesting efficiency, energy gap and exciton binding energy. Duran Karakaş: The modelling of $Pt(B^1)_2$, $Pt(B^2)_2$ and $Pt(B^3)_2$ complexes and the calculation of optimized molecular structures, spectroscopic properties (IR, ^{1}H-NMR, UV–Vis) and interpretation of all calculation results and writing of the article.

Declaration of Competing Interest

The authors declare that they have no known competing financial interests or personal relationships that could have appeared to influence the work reported in this paper.

Data Availability

Data will be made available on request.

References

[1] C.M. Da Silva, D.L. da Silva, L.V. Modolo, R.B. Alves, M.A. de Resende, C. V. Martins, Â. de Fátima, Schiff bases: a short review of their antimicrobial activities, J. Adv. Res. 2 (1) (2011) 1–8.
[2] D. Wu, L. Guo, S.J. Li, Synthesis, structural characterization and anti-breast cancer activity evaluation of three new Schiff base metal (II) complexes and their nanoparticles, J. Mol. Struct. 1199 (2020), 126938.
[3] P. Ghorai, R. Saha, S. Bhuiya, S. Das, P. Brandão, D. Ghosh, A. Saha, Syntheses of Zn (II) and Cu (II) Schiff base complexes using N, O donor Schiff base ligand: crystal structure, DNA binding, DNA cleavage, docking and DFT study, Polyhedron 141 (2018) 153–163.
[4] P. Przybylski, A. Huczynski, K. Pyta, B. Brzezinski, F. Bartl, Biological properties of Schiff bases and azo derivatives of phenols, Curr. Org. Chem. 13 (2) (2009) 124–148.
[5] A.W. Tai, E.J. Lien, M.M. Lai, T.A. Khwaja, Novel N-hydroxyuanidine derivatives as anticancer and antiviral agents, J. Med. Chem. 27 (2) (1984) 236–238.
[6] P.H. Wang, J.G. Keck, E.J. Lien, M.M. Lai, Design, synthesis, testing, and quantitative structure-activity relationship analysis of substituted salicylaldehyde Schiff bases of 1-amino-3-hydroxyguanidine tosylate as new antiviral agents against coronavirus, J. Med. Chem. 33 (2) (1990) 608–614.
[7] Z. Gul, N.U. Din, E. Khan, F. Ullah, M.N. Tahir, Synthesis, molecular structure, antimicrobial, anti-oxidant and enzyme inhibition activities of 2-amino-6-methylbenzothiazole and its Cu (II) and Ag (I) complexes, J. Mol. Struct. 1199 (2020), 126956.
[8] C. Gennari, U. Piarulli, Combinatorial libraries of chiral ligands for enantioselective catalysis, Chem. Rev. 103 (8) (2003) 3071–3100.
[9] B.M. Cole, K.D. Shimizu, C.A. Krueger, J.P. Harrity, M.L. Snapper, A.H. Hoveyda, Discovery of chiral catalysts through ligand diversity: Ti-catalyzed enantioselective addition of TMSCN to meso epoxides, Angew. Chem. Int. Ed. Engl. 35 (15) (1996) 1668–1671.
[10] H. Brunner, M. Weber, M. Zabel, [(Cy) Ru (LL*) Cl] and related half-sandwich compounds—two diastereomers in the same single crystal, Coord. Chem. Rev. 242 (1–2) (2003) 3–13.
[11] R. Drozdzak, B. Allaert, N. Ledoux, I. Dragutan, V. Dragutan, F. Verpoort, Ruthenium complexes bearing bidentate Schiff base ligands as efficient catalysts for organic and polymer syntheses, Coord. Chem. Rev. 249 (24) (2005) 3055–3074.
[12] M. Ramesh, G. Venkatachalam, New five coordinate Ru (II) carbonyl complexes containing 2–aminofluorene schiff base derivatives: synthesis, structure and catalytic activity, ChemistrySelect 3 (31) (2018) 9056–9061.
[13] L.H. Abdel-Rahman, A.M. Abu-Dief, H. Moustafa, A.A.H. Abdel-Mawgoud, Design and nonlinear optical properties (NLO) using DFT approach of new Cr (III), VO (II), and Ni (II) chelates incorporating tri-dentate imine ligand for DNA interaction, antimicrobial, anticancer activities and molecular docking studies, Arab. J. Chem. 13 (1) (2020) 649–670.

[14] D. Sajan, H. Joe, V.S. Jayakumar, J. Zaleski, Structural and electronic contributions to hyperpolarizability in methyl p-hydroxy benzoate, J. Mol. Struct. 785 (1–3) (2006) 43–53.
[15] K.S. Thanthiriwatte, K.N. De Silva, Non-linear optical properties of novel fluorenyl derivatives—ab initio quantum chemical calculations, J. Mol. Struct.: THEOCHEM 617 (1–3) (2002) 169–175.
[16] R.G. Pearson, Absolute electronegativity and hardness correlated with molecular orbital theory, Proc. Natl. Acad. Sci. 83 (22) (1986) 8440–8441.
[17] M. Odabaşoğlu, Ç. Albayrak, B. Koşar, O. Büyükgüngör, Synthesis, spectroscopic characterizations and quantum chemical computational studies of (*Z*)-4-[(*E*)-p-tolyldiazenyl]-6-[(2-hydroxyphenylamino) methylene]-2-methoxycyclohexa-2, 4-dienone, Spectrochim. Acta Part A: Mol. Biomol. Spectrosc. 92 (2012) 357–364.
[18] N. Özkan, S. Erkan, K. Sayın, D. Karakaş, Research on structural, spectral (IR, UV-Vis, 1H-and 13C-NMR) and light emitting properties of triisocyano-based trinuclear Au (I) complexes, Chem. Pap. 74 (8) (2020) 2415–2425.
[19] J. Shi, W. Zhao, L. Xu, Y. Kan, C. Li, J. Song, H. Wang, Small molecules of cyclopentadithiophene derivatives: effect of sulfur atom position and substituted groups on their UV–Abs properties, J. Phys. Chem. C 118 (15) (2014) 7844–7855.
[20] A. Karimata, S. Suzuki, M. Kozaki, K. Kimoto, K. Nozaki, H. Matsushita, K. Okada, Direct observation of hole shift and characterization of spin states in radical ion pairs generated from photoinduced electron transfer of (Phenothiazine) n–anthraquinone (n= 1, 3) Dyads, J. Phys. Chem. A 118 (47) (2014) 11262–11271.
[21] R. Zaier, S. Hajaji, M. Kozaki, S. Ayachi, DFT and TD-DFT studies on the electronic and optical properties of linear π-conjugated cyclopentadithiophene (CPDT) dimer for efficient blue OLED, Opt. Mater. 91 (2019) 108–114.
[22] D. Karakaş, S.E. Kariper, Theoretical investigation on the vibrational and electronic spectra of three isomeric forms of dicobalt octacarbonyl, J. Mol. Struct. 1062 (2014) 77–81.
[23] M. Wright, A. Uddin, Solar energy materials & solar cells organic—inorganic hybrid solar cells: a comparative review, Sol. Energy Mater. Sol. Cells 107 (2012) 87–111.
[24] J. Gong, K. Sumathy, Q. Qiao, Z. Zhou, Review on dye-sensitized solar cells (DSSCs): advanced techniques and research trends, Renew. Sustain. Energy Rev. 68 (2017) 234–246.
[25] Dennington, R.D.I.I., Keith, T.A., Millam, J.M. (2016). GaussView, version 6.0. 16. Semichem Inc Shawnee Mission KS.
[26] A.K. Rappé, C.J. Casewit, K.S. Colwell, W.A. Goddard III, W.M. Skiff, UFF, a full periodic table force field for molecular mechanics and molecular dynamics simulations, J. Am. Chem. Soc. 114 (25) (1992) 10024–10035.
[27] Frisch, M.J., Trucks, G.W., Schlegel, H.B., Scuseria, G.E., Robb, M.A., Cheeseman, J.R., Fox, D.J. (2016). Gaussian 16 Revision C. 01. 2016; Gaussian Inc. Wallingford CT, 421.
[28] Ş. Güveli, N. Özdemir, T. Bal-Demirci, B. Ülküseven, M. Dinçer, Ö. Andaç, Quantum-chemical, spectroscopic and X-ray diffraction studies on nickel complex of 2-hydroxyacetophenone thiosemicarbazone with triphenylphospine, Polyhedron 29 (12) (2010) 2393–2403.
[29] J. Gauss, GIAO-MBPT (3) and GIAO-SDQ-MBPT (4) calculations of nuclear magnetic shielding constants, Chem. Phys. Lett. 229 (3) (1994) 198–203.
[30] A.D. Becke, Density-functional exchange-energy approximation with correct asymptotic behavior, Phys. Rev. A 38 (6) (1988) 3098.
[31] Rassolov, V.A., Ratner, M.A., Pople, J.A., Redfern, P.C., Curtiss, L.A. (2001). 6–31G* basis set for third-row atoms. Journal of Computational Chemistry, 22(9), 976–984.
[32] A. Popczyk, A. Aamoum, A. Migalska-Zalas, P. Płóciennik, A. Zawadzka, J. Mysliwiec, B. Sahraoui, Selected organometallic compounds for third order nonlinear optical application, Nanomaterials 9 (2) (2019) 254.
[33] Z.X. Chen, J.M. Xiao, H.M. Xiao, Y.N. Chiu, Studies on heats of formation for tetrazole derivatives with density functional theory B3LYP method, J. Phys. Chem. A 103 (40) (1999) 8062–8066.
[34] X.X. Zhang, M. Bao, N. Pan, Y.X. Zhang, J.Z. Jiang, IR and raman vibrational assignments for metal-free phthalocyanine from density functional B3LYP/6–31G (d) method, Chin. J. Chem. 22 (4) (2004) 325–332.
[35] S. Kaya, S. Erkan, D. Karakaş, Computational design and characterization of platinum-II complexes of some Schiff bases and investigation of their anticancer–antibacterial properties, Appl. Organomet. Chem. 36 (9) (2022), e6805.
[36] I.M. Alecu, J. Zheng, Y. Zhao, D.G. Truhlar, Computational thermochemistry: scale factor databases and scale factors for vibrational frequencies obtained from electronic model chemistries, J. Chem. Theory Comput. 6 (9) (2010) 2872–2887.
[37] O.A. Ali, L.H. Abdel-Rahman, R.M. Ramadan, Ruthenium carbonyl derivatives of N-salicylidene-2-hydroxyaniline, J. Coord. Chem. 60 (21) (2007) 2335–2342.
[38] J.S. Rani, U.R. Felscia, S.N. Eastman, D. Yamini, Theoretical investigations on structural, optical and vibrational properties of pyridine 3-carboxylic acid adsorbed on a silver cluster, J. Electron. Mater. 51 (7) (2022) 3970–3979.
[39] S. Sebastian, N. Sundaraganesan, The spectroscopic (FT-IR, FT-IR gas phase, FT-Raman and UV) and NBO analysis of 4-Hydroxypiperidine by density functional method, Spectrochim. Acta Part A Mol. Biomol. Spectrosc. 75 (3) (2010) 941–952.
[40] Y. Shen, X. Li, J. Ye, Y. Qiu, A DFT study on second-order NLO properties of bis-cyclometalated Iridium (III) complexes with chelating dicarbene auxiliary ligands, Comput. Theor. Chem. 1163 (2019), 112535.
[41] P. Rawat, R.N. Singh, Experimental and theoretical study of 4-formyl pyrrole derived aroylhydrazones, J. Mol. Struct. 1084 (2015) 326–339.
[42] S. Erkan, D. Karakaş, Computational investigation of structural, nonlinear optical and anti-tumor properties of dinuclear metal carbonyls bridged by pyridyl ligands with alkyne unit, J. Mol. Struct. 1199 (2020), 127054.
[43] M.B. Oviedo, N.V. Ilawe, B.M. Wong, Polarizabilities of π-conjugated chains revisited: improved results from broken-symmetry range-separated DFT and new CCSD (T) benchmarks, J. Chem. Theory Comput. 12 (8) (2016) 3593–3602.
[44] M.E. Foster, B.M. Wong, Nonempirically tuned range-separated DFT accurately predicts both fundamental and excitation gaps in DNA and RNA nucleobases, J. Chem. Theory Comput. 8 (8) (2012) 2682–2687.
[45] Y.K. Lan, C.I. Huang, A theoretical study of the charge transfer behavior of the highly regioregular poly-3-hexylthiophene in the ordered state, J. Phys. Chem. B 112 (47) (2008) 14857–14862.
[46] H.S. Ren, M.J. Ming, J.Y. Ma, X.Y. Li, Theoretical calculation of reorganization energy for electron self-exchange reaction by constrained density functional theory and constrained equilibrium thermodynamics, J. Phys. Chem. A 117 (33) (2013) 8017–8025.
[47] F. Sun, R. Jin, DFT and TD-DFT study on the optical and electronic properties of derivatives of 1, 4-bis (2-substituted-1, 3, 4-oxadiazole) benzene, Arab. J. Chem. 10 (2017) S2988–S2993.
[48] S. Negi, P. Mittal, B. Kumar, Impact of different layers on performance of OLED, Microsyst. Technol. 24 (2018) 4981–4989.
[49] A. Lukyanov, C. Lennartz, D. Andrienko, Amorphous films of tris (8–hydroxyquinolinato) aluminium: force-field, morphology, and charge transport, Phys. Status Solidi (a) 206 (12) (2009) 2737–2742.
[50] B.C. Lin, C.P. Cheng, Z.P.M. Lao, Reorganization energies in the transports of holes and electrons in organic amines in organic electroluminescence studied by density functional theory, J. Phys. Chem. A 107 (26) (2003) 5241–5251.
[51] J.D. Thompson, P. Winget, D.G. Truhlar, MIDIX basis set for the lithium atom: accurate geometries and atomic partial charges for lithium compounds with minimal computational cost, PhysChemComm 4 (16) (2001) 72–77.
[52] U. Daswani, U. Singh, P. Sharma, A. Kumar, From molecules to devices: a DFT/TD-DFT study of dipole moment and internal reorganization energies in optoelectronically active aryl azo chromophores, J. Phys. Chem. C 122 (26) (2018) 14390–14401.
[53] M.I. Khan, J. Iqbal, S.J. Akram, Y.A. El-Badry, M. Yaseen, R.A. Khera, End-capped group modification on cyclopentadithiophene based non-fullerene small molecule acceptors for efficient organic solar cells; a DFT approach, J. Mol. Graph. Model. 113 (2022), 108162.
[54] M.A. Sakr, F.F. Sherbiny, A.A.S. El-Etrawy, Hydrazone-based materials; DFT, TD-DFT, NBO analysis, fukui function, MESP analysis, and solar cell applications, J. Fluoresc. 32 (5) (2022) 1857–1871.
[55] S. Bedoura, H.W. Xi, H.W. Goh, K.H. Lim, DFT/TDDFT Investigation on donor-acceptor triazole-based copolymers for organic photovoltaics, J. Mol. Struct. 1248 (2022), 131406.
[56] M.R.S.A. Janjua, Photovoltaic properties and enhancement in near-infrared light absorption capabilities of acceptor materials for organic solar cell applications: a quantum chemical perspective via DFT, J. Phys. Chem. Solids 171 (2022), 110996.
[57] M. Bourass, A.T. Benjelloun, M. Benzakour, M. Mcharfi, M. Hamidi, S.M. Bouzzine, M. Bouachrine, DFT and TD-DFT calculation of new thienopyrazine-based small molecules for organic solar cells, Chem. Cent. J. 10 (1) (2016) 1–11.
[58] Casida, M.E.. (1995). Time-dependent density functional response theory for molecules. In Recent Advances In Density Functional Methods: (Part I) (pp. 155–192).